*International Research Journal of Environmental Sciences*_____ ISSN 2319–1414
Vol. **15(4),** 106-111, October **(2026)** *Int. Res. J. Environmental Sci.*

Assessment of Stormwater accumulation and Urban Flood Hazard in Samarkand City Using Remote Sensing, GIS Technologies and the SWMM Model

Manuchekhr Khaydarovich Bobokalonov
Samarkand State Technical University, Lolazor Street, Samarkand 140143, Uzbekistan
ilmiyizlanuvchi@gmail.com

Available online at: www.isca.in, www.isca.me
Received 23rd September 2026, revised 10th October 2026, accepted 21st October 2026

Abstract

Rapid urban expansion, increasing impervious cover and the growing variability of precipitation make stormwater management a pressing issue for the cities of Central Asia. This study assesses stormwater accumulation and the resulting flood hazard in Samarkand city (Uzbekistan) by integrating satellite remote sensing data, GIS-based spatial analysis and the EPA Storm Water Management Model (SWMM). Land cover, imperviousness and surface topography derived from remote sensing products were used to delineate urban subcatchments and parameterise the hydrological model. Four design-storm scenarios of 120 minutes duration were generated with the Alternating Block Method (ABM); peak intensities ranged from about 102 to 120 mm/h. The 2025 climatic record shows a strongly seasonal regime: roughly 285 mm of annual precipitation, of which about 91% fell between December and May, and a single month (December) contributed about 35% of the annual total. Modelled flood hazard was classified into five classes (very low to very high). Under the least severe scenario, high and very high hazard zones covered about 9% of the study area, rising to about 32% under the most severe scenario, while the very high class grew from about 1% to 15%. The results demonstrate that a combined RS-GIS-SWMM workflow is an effective and low-cost tool for identifying drainage bottlenecks and prioritising stormwater infrastructure and low-impact development (LID) measures in semi-arid cities.

Keywords: Stormwater, SWMM, remote sensing, GIS, urban flooding, design storm, Alternating Block Method, Samarkand.

Introduction

Urban flooding is among the most frequent and costly natural hazards worldwide and its assessment increasingly relies on remotely sensed data[1]. In cities, the replacement of vegetated and permeable surfaces by roofs, roads and paved areas reduces infiltration, shortens the time of concentration and increases both peak discharge and runoff volume, so that growing imperviousness raises flood risk[2]. Semi-arid and continental regions are particularly vulnerable because short, intense rainfall events fall on dry, crusted or sealed surfaces and on drainage networks that were often designed for lower design intensities.

Process-based hydrological-hydraulic models are the standard tool for analysing such problems. The Storm Water Management Model (SWMM), developed by the U.S. Environmental Protection Agency, simulates rainfall-runoff, infiltration, surface routing and flow in conduits and nodes, and is widely used for drainage design, flood assessment and the evaluation of LID practices[3]. Its main limitation is its demand for spatially distributed input parameters such as catchment area, slope, width, imperviousness and roughness. Remote sensing (RS) and geographic information systems (GIS) fill this gap: multispectral imagery provides land cover and impervious surface fractions, digital elevation models (DEMs) provide slope and flow direction, and GIS tools automate catchment delineation and parameter extraction[2,4]. The combination of SWMM with GIS has been applied to campus drainage analysis under design storms in India[5] and to ward-scale planning of blue-green infrastructure in Mumbai[6], while hydrological and hydraulic models coupled with GIS have likewise been used to simulate floods and to prepare flood hazard maps[7,8].

Samarkand, one of the oldest and most historically significant cities of Uzbekistan, has experienced considerable urban growth and densification. Winter-spring rainfall events and occasional intense storms cause water to accumulate on roads and in low-lying neighborhoods. Recent work in the Samarkand region has examined the effect of urban expansion on groundwater and the choice of structural and non-structural flood protection measures[9], but a systematic, model-based assessment of stormwater accumulation in the city is still lacking.

The objectives of this study are: i. to characterise the climatic and precipitation regime of the study area; ii. to derive SWMM input parameters from RS and GIS data; iii. to generate design hyetographs using the Alternating Block Method; and iv. to evaluate the spatial distribution of flood hazard classes under four storm scenarios.

Study Area and Climate: Samarkand is located in the Zarafshan River valley in south-eastern Uzbekistan at elevations

of about 646-818 m a.s.l. within the city boundary (Figure-1; approx. 39.6° N, 67.0° E). The climate is continental and semi-arid, with hot, dry summers and cool, wetter winters and springs. Precipitation is concentrated in the cold half of the year, while the summer months are almost rainless. Elevation is lowest in the northern part of the city and rises towards the south and east, where a compact elevated area exceeds 758 m. This topographic gradient controls surface flow paths and the location of natural low points where stormwater accumulates, and it underlies the subcatchment delineation described in Section 3.2.

Figure-2 presents the monthly temperature and precipitation for 2025, and Table-1 summarises the values read from the climograph.

The annual precipitation total is approximately 285 mm. The precipitation regime is markedly uneven: December to May accounts for about 258 mm (≈91%), whereas June to September together contribute only about 3.5 mm (≈1%). December 2025 was exceptional, with about 99 mm, more than twice the next wettest month (March). Because December temperatures were low (≈4-5 °C) and evapotranspiration is minimal, such a month produces wet antecedent conditions and a high likelihood of runoff and surface ponding. The mean temperature curve peaks in July (≈28.5 °C) and reaches its minimum in January (≈0.5 °C), confirming the continental character of the climate.

Methodology

Data sources: The input data used in the study, together with their sources and purposes, are listed in Table-2. Satellite imagery and the DEM supplied the land cover and topographic information, the 2025 monthly climatic record (Table-1) described the precipitation regime, and the design hyetographs (Figure-3) provided the rainfall input to SWMM.

Table-1: Monthly climate characteristics of the study area, 2025 (values read from Figure-2; approximate).

Month	Precipitation (mm)	Share of annual total (%)	Mean temperature (°C)
January	29	10.2	0.5
February	37	13.0	2.5
March	45	15.8	7.5
April	34	11.9	16.0
May	14	4.9	22.0
June	2	0.7	25.5
July	1.5	0.5	28.5
August	~0	~0	26.0
September	~0	~0	21.0
October	7	2.5	15.5
November	16	5.6	7.5
December	99	34.8	4.5
Year	≈285	100	≈14.8 (mean)

Table-2: Input data used in the study.

Data type	Source / product	Purpose
Multispectral satellite imagery	Satellite remote sensing products	Land cover classification, NDVI, NDBI, imperviousness
Digital elevation model	Digital elevation data	Slope, flow direction, subcatchment delineation
Meteorological data	Monthly temperature and precipitation, 2025 (Table-1)	Climatic characterisation, antecedent conditions
Rainfall design data	Alternating Block Method hyetographs (Figure-3)	SWMM rainfall input
Drainage network and roads	Drainage network and road data	Conduits, nodes and outfalls
Soil data	Soil data	Infiltration parameters

Remote sensing and GIS processing: Satellite images were pre-processed (atmospheric and radiometric correction, cloud masking, clipping to the city boundary). Land cover was classified into built-up, road/paved, bare soil, vegetation and water classes using a supervised classifier trained on reference samples, and accuracy was verified by a confusion matrix. Spectral indices supported the classification: the Normalised Difference Vegetation Index, NDVI[10], the Normalised Difference Built-up Index, NDBI, and the Normalised Difference Water Index, NDWI[11]. The percentage of impervious area in each subcatchment was calculated by combining the built-up, road and paved classes.

The DEM was hydrologically conditioned (sink filling), after which flow direction and flow accumulation were computed. The study area was divided into subcatchments, and for each of them area, average slope, characteristic flow width and impervious percentage were extracted using GIS zonal statistics.

Design storm: Alternating Block Method: Design rainfall was generated from intensity-duration-frequency (IDF) relationships using the Alternating Block Method[12], a procedure related to the earlier Chicago-type synthetic storm pattern[13]. Intensities for successive time increments (here $\Delta t = 5$ min) were computed from the IDF curve, converted to incremental depths, and the blocks were rearranged so that the maximum block is placed near the middle of the storm and the remaining blocks alternate to its right and left in descending order. The total storm duration was 120 min. Four scenarios of increasing severity were produced, and the hyetograph of the first scenario is shown in Figure-3.

SWMM set-up: SWMM 5 was used to simulate rainfall-runoff and flow routing. Surface runoff was computed with the non-linear reservoir approach, infiltration with a standard infiltration method, and flow routing with the dynamic wave equations. Initial parameter values were taken from SWMM guidance and the literature and refined using GIS-derived characteristics; the principal parameters and their sources are given in Table-3.

Flood hazard classification: Simulated flooding at nodes and ponding on subcatchments (maximum flood depth, flood duration and flooded volume) was combined with surface topography and land use in GIS, in line with the approach of coupling hydrological and hydraulic outputs with GIS for hazard mapping[8]. The resulting hazard index was divided into five classes: very low, low, medium, high and very high. The share of the study area falling into each class was calculated for every scenario.

Figure-4 summarises the workflow: remote sensing and GIS processing turn raw inputs into SWMM parameters, SWMM simulates the four storm scenarios, and its flood output is classified into hazard classes that point to priority areas for drainage upgrades and LID measures.

Results and Discussion

Design storm characteristics: Figure-3 shows that all four hyetographs share the same symmetrical-peaked shape imposed by the ABM. Intensities in the first 40 minutes are low and increase slowly, from about 5 mm/h at the start to about 10-14 mm/h around minute 40-45. A single sharp peak occurs at approximately minute 55, followed by a rapid recession to about 30 mm/h in the next interval and a long tail of about 4-5 mm/h at the end of the 120-minute event. The peak intensity, the time of the peak and the intensity of the block after the peak for each scenario series are given in Table-4.

The peak block exceeds the neighboring blocks by a factor of 4-5. For the highest series, the sum of all blocks corresponds to a total storm depth of the order of 28 mm in two hours (graphical estimate), of which the peak 5-minute block alone represents about 10 mm. Such a short, intense burst is typical of convective storms and is critical for urban drainage because it can exceed the infiltration capacity of soils and the inlet capacity of storm drains within minutes. Note that the ABM concentrates the rainfall around one peak, which is a conservative assumption and tends to produce higher peak discharges than real, temporally variable storms.

Table-3: Principal SWMM parameters and their source (typical literature ranges)[3].

Parameter	Typical value / range	Source /References
Subcatchment area (ha)	from GIS	DEM delineation
Average slope (%)	from GIS	DEM
Imperviousness (%)	from RS	Land cover classification
Manning's n, impervious surface	0.011-0.015	3
Manning's n, pervious surface	0.10-0.40	3
Depression storage, impervious (mm)	1.3-2.5	3
Depression storage, pervious (mm)	2.5-7.5	3
Conduit roughness (Manning's n)	0.011-0.015	Pipe material
Time step (routing)	1-5 s	Numerical stability

Table-4: Characteristics of the design hyetographs read from Figure-3 (approximate).

Scenario series (legend index)	Peak intensity (mm/h)	Approx. time of peak (min)	Intensity in the block after the peak (mm/h)
Series 0	≈120	55	≈31
Series 1	≈109	55	≈28
Series 2	≈105	55	≈27
Series 3	≈102	55	≈26

Table-5: Share of the study area by flood hazard class (%) (approximate values read from Figure-5).

Hazard class	Scenario 1	Scenario 2	Scenario 3	Scenario 4
Very low	3.0	3.5	3.8	4.2
Low	43.7	33.2	29.0	25.0
Medium	44.2	44.8	41.8	38.5
High	8.3	11.0	14.0	17.0
Very high	1.0	7.4	11.0	15.0

Table-6: Aggregated hazard indicators derived from Table-5 (%).

Indicator	Scenario 1	Scenario 2	Scenario 3	Scenario 4
Very low + low	46.7	36.7	32.8	29.2
Medium	44.2	44.8	41.8	38.5
High + very high	9.3	18.4	25.0	32.0
Change in high + very high relative to Scenario 1 (percentage points)	-	+9.1	+15.7	+22.7

Spatial distribution of flood hazard: Figure-5 and Table-5 present the share of the study area in each hazard class under the four scenarios, and Table 6 aggregates these shares into broader indicators.

Three patterns emerge. First, the low-hazard class shrinks consistently from about 44% to about 25%, indicating that the more severe scenarios convert large parts of the formerly safe area into medium and higher hazard. Second, the medium class is the largest or second-largest class in all scenarios (≈39-45%) and acts as a transition zone: it gains area from the low class but loses area to the high classes under the more severe scenarios. Third, the very high class shows the strongest response: it grows from about 1% in Scenario 1 to about 7% in Scenario 2 and 15% in Scenario 4, i.e. a fifteen-fold increase. The combined high and very high share increases from roughly 9% to 32%, so the area exposed to serious flooding more than triples.

The non-linear response of the very high class suggests that threshold effects exist in the drainage system: once the capacity of conduits and inlets in low-lying subcatchments is exceeded, surcharge and surface ponding expand rapidly. Such areas are typically characterised by high imperviousness, gentle slopes and limited drainage capacity, and they represent priority locations for intervention.

Interaction of climate regime and flood hazard: The climatic data (Table 1) indicate that the highest runoff risk is associated with the cold season. December 2025 (≈99 mm) and the March peak (≈45 mm) occur when evapotranspiration is low and soils are often wet or semi-frozen, so that the effective infiltration capacity is reduced. In contrast, summer storms, although rare, may be very intense and fall on dry, crusted and impervious surfaces. The drainage system must therefore cope with two distinct flood-generating mechanisms: prolonged, wet-season rainfall and short, high-intensity convective events. The design hyetographs in Figure-3 represent the second mechanism, while the monthly record represents the first.

Implications for stormwater management: The results support the following priorities: (i) upgrading or supplementing drainage capacity in sub catchments classified as high or very high hazard; (ii) reducing runoff generation through LID measures (permeable pavements, bioswales, green roofs, retention basins) where imperviousness is highest, an approach whose ability to lower peak runoff and peak flooding has been demonstrated by SWMM-based studies elsewhere[6]; (iii) preserving natural drainage paths and green areas that function as retention zones; and (iv) maintaining inlets and channels before the wet season (November-December). Because the hazard area expands markedly between scenarios, design

standards based only on low-return-period storms may leave a large part of the city under-protected.

Limitations: The values in Tables-1, 4, 5 and 6 were digitised from graphs and are therefore approximate. Coarse-resolution DEMs may misrepresent micro-topography and street-level flow paths. Impervious area from medium-resolution imagery is subject to classification uncertainty and mixed pixels. The ABM design storm is a synthetic event and does not reproduce observed rainfall variability, and SWMM results depend on the quality of drainage network data and calibration. Calibration and validation against observed flood records or flow measurements (e.g. Nash-Sutcliffe efficiency, peak-flow error) remain a priority for future work.

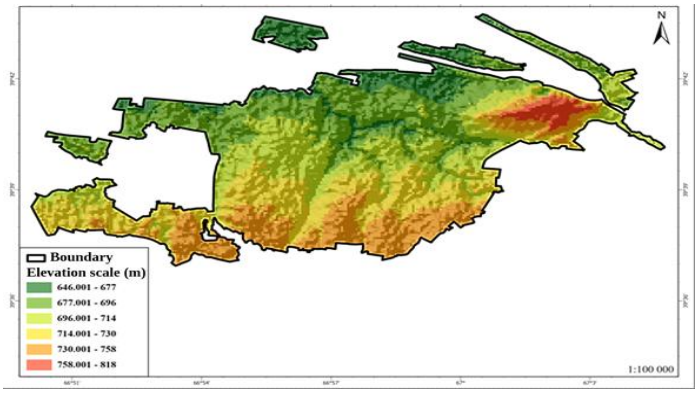


Figure-1: Relief map of Samarkand city derived from the DEM (elevation 646-818 m a.s.l., scale 1:100 000).

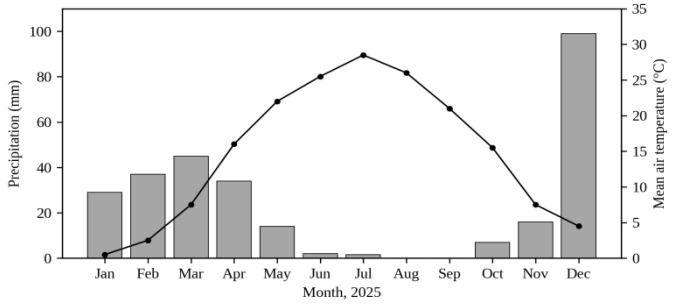


Figure-2: Monthly precipitation (bars) and mean air temperature (line), 2025, plotted from the values in Table-1.

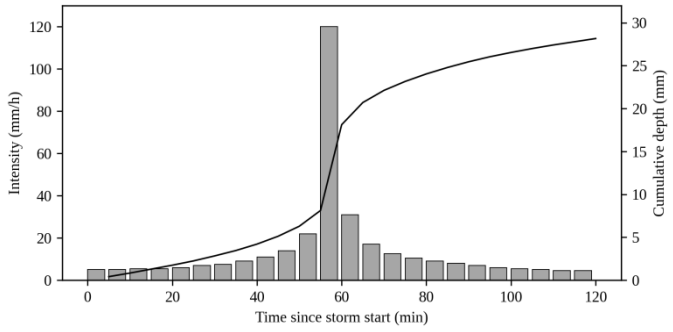


Figure-3: Design hyetograph generated by the Alternating Block Method (5-min step, 120 min) with its cumulative depth. Series 0 is shown; the other three series have the same shape with peaks of about 109, 105 and 102 mm/h.

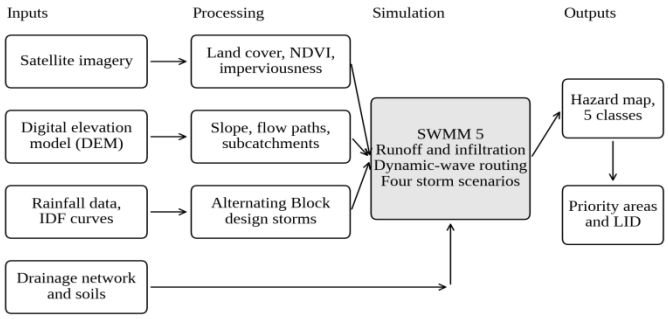


Figure-4: Workflow of the integrated RS-GIS-SWMM assessment.

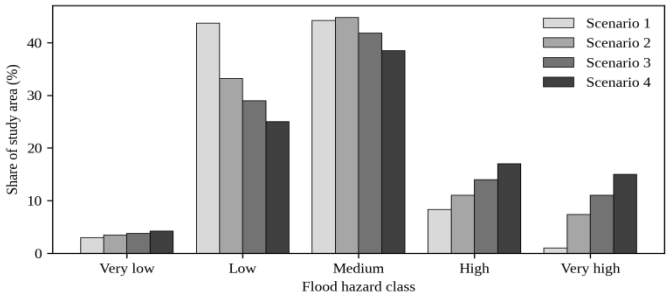


Figure-5: Distribution of the study area by flood hazard class for the four scenarios (Table-5).

Conclusion

The 2025 climatic record shows a highly seasonal regime with about 285 mm of annual precipitation, ≈91% of it between December and May, and an exceptional December (≈99 mm, ≈35% of the annual total). The Alternating Block Method produced 120-minute design storms with a single sharp peak at about minute 55 and peak intensities of about 102-120 mm/h, which are sufficient to overload urban drainage elements. The share of the study area under high and very high flood hazard increased from about 9% to about 32% across the scenarios, while the very high class increased from about 1% to 15%.

Integrating RS, GIS and SWMM provides a reproducible, data-efficient workflow for locating flood-prone areas and for prioritising drainage upgrades and LID measures in Samarkand and in comparable semi-arid cities. Future work should include calibration with observed flow or flood-extent data, higher-resolution DEM and drainage inventories, and the simulation of specific LID scenarios and climate-change-adjusted rainfall.

References

1. Taubenböck, H., Wurm, M., Netzband, M., Zwenzner, H., Roth, A., Rahman, A., & Dech, S. (2011). Flood risks in urbanized areas - multi-sensoral approaches using remotely

sensed data for risk assessment. *Natural Hazards and Earth System Sciences*, 11(2), 431-444.

2. Dang, A. T. N. & Kumar, L. (2017). Application of remote sensing and GIS-based hydrological modelling for flood risk analysis: a case study of District 8, Ho Chi Minh city, Vietnam. *Geomatics, Natural Hazards and Risk*, 8(2), 1792-1811.

3. Rossman, L. A. (2015). Storm Water Management Model. User's Manual, Version 5.1. EPA/600/R-14/413b. U.S. Environmental Protection Agency, Cincinnati, OH.

4. Pawar, U., Suppawimut, W., Muttil, N. & Rathnayake, U. (2022). A GIS-based comparative analysis of frequency ratio and statistical index models for flood susceptibility mapping in the Upper Krishna Basin, India. *Water*, 14(22), 3771.

5. Rangari, V. A., Prashanth, S., Umamahesh, N. V. & Patel, A. K. (2018). Simulation of urban drainage system using a Storm Water Management Model (SWMM). *Asian Journal of Engineering and Applied Technology*, 7(S1), 7-10.

6. Kelkar, V., Solanki, V. & Krebs, P. (2026). SWMM-based hydrological modelling of blue-green infrastructure for climate-resilient stormwater management and urban flood reduction under the 25-year return period extreme rainfall scenario in F-North and G-North wards of Greater Mumbai, India. *Water*, 18(13), 1542.

7. Hashemyan, F., Khaleghi, M. R., & Kamyar, M. (2015). Combination of HEC-HMS and HEC-RAS models in GIS in order to simulate flood (Case study: Khoshke Rudan River in Fars Province, Iran). Res. J. Recent Sci., 4(8), 122-127.

8. Peker, İ. B., Gülbaz, S., Demir, V., Orhan, O. & Beden, N. (2024). Integration of HEC-RAS and HEC-HMS with GIS in flood modeling and flood hazard mapping. *Sustainability*, 16(3), 1226.

9. Tadzhibaeva, N., Stelmakh, A., Abdullaeva, M., Kurbonova, M. & Mirfayziyeva, F. (2026). Land reclamation and natural resource management in the Samarkand region, Uzbekistan. E3S Web of Conferences, 703, 03007.

10. Tucker, C. J. (1979). Red and photographic infrared linear combinations for monitoring vegetation. *Remote Sensing of Environment*, 8(2), 127-150.

11. McFeeters, S. K. (1996). The use of the Normalized Difference Water Index (NDWI) in the delineation of open water features. *International Journal of Remote Sensing*, 17(7), 1425-1432.

12. Chow, V. T., Maidment, D. R. & Mays, L. W. (1988). Applied Hydrology. McGraw-Hill, New York.

13. Keifer, C. J., & Chu, H. H. (1957). Synthetic storm pattern for drainage design. *Journal of the Hydraulics Division*, ASCE, 83(4), 1-25.